ORIGINAL PAPER

Evidence of Room Temperature Ferromagnetism in $Zn_{1-x}Sn_xS$ Thin Films

K. Chaitanya Kumar[1] · S. Kaleemulla[2] · C. Krishnamoorthi[3] · N. Madhusudhana Rao[4] · G. Venugopal Rao[5]

Abstract

Tin (Sn)-doped zinc sulfide ($Zn_{1-x}Sn_xS$) thin films at different tin (Sn) concentrations (= 0.00, 0.02, 0.05, and 0.08) were coated onto Corning 7059 glass substrates using the electron beam evaporation technique. The films were subjected to different characterization techniques to study the physical properties of the thin films. The structural properties of the films were studied using a powder X-ray diffractometer (XRD), and it was found that the films were cubic in structure without any impurity phases. The crystallite size increased with an increase of Sn concentration, and the mean crystallite size was 21 nm. The chemical composition and surface morphology of the films were studied using scanning electron microscopy (FE-SEM) with energy-dispersive analysis of X-rays (EDAX). Optical properties such as transmittance and absorbance were recorded using a diffuse reflectance spectroscope (UV–vis–NIR). All the films exhibited high optical transmittance of 85% in the visible region of the solar spectrum. The band gap of the films was calculated using Tauc's relation, and it was found that it increased from 3.53 to 3.57 eV with an increase in the Sn doping concentration from $x = 0.02$ to $x = 0.08$. The room temperature photoluminescence studies of the films were recorded using a fluorescence spectrophotometer, and it was found that the films exhibited a prominent emission peak at 420 nm. The magnetic properties of the films and glass substrates at room temperature were studied using a vibrating sample magnetometer. From this, it was found that the films were weakly ferromagnetic at room temperature and the strength of magnetization increased with an increase of doping concentration from $x = 0.02$ to $x = 0.05$ and decreased at higher doping concentrations ($x = 0.08$). The films showed high magnetization at $x = 0.05$. The films at $x = 0.05$ exhibited the magnetization (M_s), retentivity (M_r), and coercive fields (H_c) 18×10^{-6} emu/cm^3, 1.6×10^{-6} emu/cm^3, and 91.80 Oe, respectively.

Keywords Thin films · Physical vapor deposition · Crystal structure · Ferromagnetism · Transmittance

1 Introduction

Currently, low-dimensional materials are finding great interest as they possess novel properties and find applications in many optoelectronic devices. In this scenario, search is being carried out to find new materials and new methods which can exhibit novel properties and future applications, such as spintronics. Dilute magnetic semiconductors (DMS) are the materials which will be best suited for future applications. The DMS materials are the ones in which both spin and charge of electrons can be utilized. The DMS materials can be prepared by adding a small quantity of either magnetic or non-magnetic impurity ions into a non-magnetic semiconductor, and it can be made into a magnetic semiconductor. Due to the peculiar properties of these DMS materials, they play an important role in many applications

✉ S. Kaleemulla
skaleemulla@gmail.com

1 Thin Films Laboratory, School of Advanced Sciences, VIT, Vellore, Vellore, 632014, Tamil Nadu, India

2 Thin Films Laboratory, Centre for Crystal Growth, VIT, Vellore, Vellore, 632014, Tamil Nadu, India

3 Centre for Nanotechnology Research, VIT, Vellore, Vellore, 632014, Tamil Nadu, India

4 Department of Physics, VIT-AP, Amaravathi, 522034, Andhra Pradesh, India

5 Materials Physics Division, Indira Gandhi Centre for Atomic Research, Kalpakkam, 603102, Tamil Nadu, India

in semiconductor device technology. In this context, GaAs and MnAs semiconductors were studied extensively, and it was reported that they act as ferromagnetic semiconductors at low temperatures. But, in view of device fabrication, it will be a great achievement if one could observe ferromagnetism at room temperature or above room temperature. Hence, continuous efforts are being put on different types of host semiconductor materials, impurities, and synthesis methods so that ferromagnetism can be observed at room temperature. Till now, magnetic properties of the II–VI semiconductors such as ZnS, ZnO, ZnSe, ZnTe, or III–V semiconductors (SiC, GaN, GaP) were studied by adding different impurity elements like manganese (Mn), iron (Fe), cobalt (Co), nickel (Ni), etc. But, among the different II–VI semiconductors, ZnS is one of the promising materials with a wide band gap of 3.6 eV [1]. Due to its wide band gap, it finds its importance in various applications such as flat panel displays, UV-light-emitting diodes, sensors, lasers, and solar cells [2–4]. Physical and chemical coatings such as pulsed laser deposition, dc and rf sputtering, spray pyrolysis, and chemical bath deposition were applied for the preparation of undoped and doped ZnS thin films [5–8]. Among the different physical vapor deposition techniques, electron beam evaporation technique is one of the promising techniques to prepare high-quality thin films. The advantages of an electron beam evaporation technique are purity of the films, good adhesion, and deposition control with less minimum wastage of the material. It is well known that the properties of the films depend on deposition parameters such as base pressure, thickness, substrate temperature, and impurity; a systematic optimization is needed in getting the desired properties of the films. Till now, the pure and impurity doped ZnS thin films were prepared by different techniques and their structural and optical properties studied. But to the best knowledge of the authors, no articles were published on the magnetic properties of the Sn-doped ZnS thin films. This motivated us to prepare the pure and Sn-doped ZnS thin films using electron beam evaporation and study the structural, chemical, surface, optical, and magnetic properties systematically using different characterization tools. Here, the dopant tin (Sn) was chosen as the ionic radius of Sn^{2+} (0.99 Å) is closely equal to the ionic radius of Zn^{2+} (0.74 A°). In order to verify the intrinsic nature of ferromagnetism in Sn-doped ZnS thin films, the concentration of dopant Sn is taken below 10 at%. The effect of Sn in the ZnS host matrix in nanopowder form has been reported in our earlier studies [9]. The same powders were taken as source target materials for thin film coating in this work. Hence, the present manuscript deals with the preparation of pure and ZnS thin films using electron beam evaporation and the effect of Sn concentration on structural,

optical, and magnetic properties of doped ZnS thin films has been studied.

2 Experimental Details

The source material of Sn-doped ZnS was prepared using the solid state reaction method. Commercially available ZnS and SnS powders (M/S Sigma-Aldrich, 99.99% pure) were taken as source materials. These powders were precisely weighed in the required ratio using a microbalance. To get homogeneity, the powder samples were mixed and ground thoroughly using an agate mortar and pestle for 16 h. The ground powder samples were sintered using a horizontal tubular microprocessor-controlled furnace and fired at 950 °C for 2 h under a pressure of 1×10^{-3} mbar using a rotary pump. The sintered samples were prepared as pellets and used as source materials for thin film preparation. The $Zn_{1-x}Sn_xS$ thin films were prepared at different Sn concentrations of = 0.00, 0.02, 0.05, and 0.08by electron beam evaporation (12A4D). The films were coated on the Corning 7059 glass substrates. The glass substrates were cleaned with acetone and running water and dried in a hot air oven. These substrates were fixed on a resistive heating substrate holder, and the temperature of the heater was maintained at 150 °C. A base pressure of 2×10^{-6} mbar was maintained in the vacuum chamber. The current for the electron beam source was maintained in the range of 10–20 mA during the coating of the films. The thickness of the films was measured using a surface profilometer and it was about 400 nm.

The deposited thin films were then subjected to different characterization techniques to study their structural, optical, surface, elemental, and magnetic properties. The structural properties of the films were studied using a powder X-ray diffractometer (Bruker, D8 Advance PXRD) in the diffraction angle (2θ) range of 20–70° with step width of 0.04°. The surface and elemental analyses were carried out using field emission scanning electron microscopy (FE-SEM) with energy-dispersive analysis of X-rays (EDAX) (OXFORD instrument, INCA Penta FET–x3). The photoluminescence spectra were recorded in the wavelength range of 350 to 500 nm with an excitation wavelength of 375 nm using a fluorescence spectrophotometer (Hitachi F7000). The optical transmittance and absorbance spectra were recorded in the wavelength range of 300–1000 nm using a UV–Vis–NIR spectrophotometer (JASCO V-670). The magnetic properties such as magnetization, retentivity, and coercive fields were studied at room temperature using a vibrating sample magnetometer (VSM, Lakeshore 7303) at the magnetic field range of ±50 kOe.

3 Results and Discussion

3.1 Structural Properties

Figure 1a shows the X-ray diffraction profiles of $Zn_{1-x}Sn_xS$ thin films at different Sn concentrations, i.e, $x = 0.00$, 0.02, 0.05, and 0.08. From the figure, it can be seen that only one diffraction peak has been observed in the films at a diffraction angle (θ) of 2°. A sharp and high intense diffraction peak was observed along the (1 1 1) plane. The same diffraction peak has been reflected for $Zn_{1-x}Sn_xS$ thin films at different Sn concentrations = 0.00, 0.02, 0.05, and 0.08. The observed diffraction peak exactly coincided with a cubic structure of ZnS (JCPDS data 79-0043). No new diffraction peak related to the impurity tin (Sn) in any form was observed even when the Sn doping concentration increased to $x = 0.08$. Further, no change in the crystal structure was observed in the $Zn_{1-x}Sn_xS$ thin films with increase of Sn concentration. It seems that the doping concentration is less than the miscibility limit of ZnS. The (1 1 1) orientation in ZnS thin films was already reported by other research groups [10–12]. The same predominant peak for the (1 1 1) plane was observed in Sn-doped ZnS nanopowders along with the (2 2 0) and (3 1 1) planes, which represents the cubic structure.

Figure 1b shows the X-ray diffraction profiles of $Zn_{1-x}Sn_xS$ thin films in the diffraction angle (2θ) range of 27 to 31°. From the figure, it is clear that a shift in diffraction peak towards lower diffraction angles was observed. Moreover, the diffraction peak becomes more broad with the increase of doping concentration which reflects the decrease in crystallite size.

The crystallite size (D) was calculated using Schere's formula for the predominant plane (1 1 1) [13]

$$D = \frac{k\lambda}{\beta \cos\theta} \qquad (1)$$

where k is a constant (0.98), λ is the wavelength of the X-rays ($\lambda = 1.5406$ Å), β is the full width at half maximum (FWHM), and θ is the diffraction angle. The crystallite size of the films decreased from 27 to 12 nm by the increase in the Sn concentration from $x = 0.02$ to $x = 0.08$. The average crystallite size found was ~21 nm. The lattice parameter of the films increased from 5.27 to 5.36 Å with the increase of dopant concentration from $x = 0.00$ to $x = 0.08$ which may be due to the difference in the ionic radii of Zn^{2+} (0.74 Å) and Sn^{2+} (0.99 Å) [14]. As the ionic radius of Zn^{2+} is less than the ionic radius of Sn^{2+}, an increase in the lattice parameter has been observed in $Zn_{1-x}Sn_xS$ thin films by an increase in Sn concentration. Similar kinds of results were also observed in Sn-doped ZnS nanoparticles [15, 16].

In order to further clarify the changes due to Sn substitution, the dislocation density and microstrains were also calculated as these are related to the misregistry of the lattice within the crystal. According to Sarmah et al. [17], the dislocation density may play a major role in the growth mechanism of thin films, which in turn effects the strain that develops in thin films. The dislocation density (δ) of the thin films was calculated using the following relation:

$$\delta = \frac{1}{D^2} \qquad (2)$$

Fig. 1 **a** X-ray diffraction patterns of $Zn_{1-x}Sn_xS$ thin films. **b** X-ray diffraction profile of $Zn_{1-x}Sn_xS$ thin films in the 2θ range of 27 to 31°
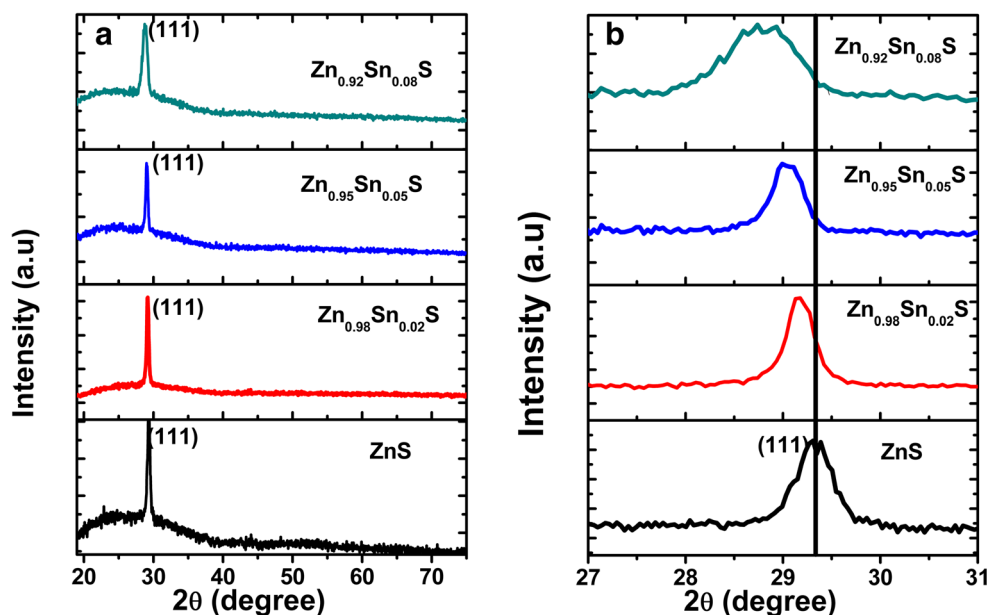
Table 1 The FWHM, crystallite size, lattice parameter, dislocation density and microstrain variations in $Zn_{1-x}Sn_xS$ thin films

$Zn_{1-x}Sn_xS$	Crystallite size (D) (nm)	FWHM	Lattice parameter (a) (Å)	Dislocation density (δ) (10^{14} m^{-2})	Strain (ε) (10^{-4} lines/cm)
$x = 0.00$	20	0.420	5.27	24	18
$x = 0.02$	27	0.310	5.29	13	13
$x = 0.05$	25	0.342	5.32	16	14
$x = 0.08$	12	0.737	5.36	80	32

where δ is the dislocation density and D is the crystallite size.

The microstrain (ε) was calculated using the following relation:

$$\varepsilon = \frac{\beta \cos \theta}{4} \tag{3}$$

where β is the full width at half maximum (FWHM) and θ is Bragg's diffraction angle. The dislocation density and microstrain increased with the increase of Sn dopant concentration. The FWHM, crystallite size, lattice parameter, dislocation density and microstrain at different doping concentrations are shown in Table 1.

The crystallinity is found to increase for Sn-doped ZnS thin films on comparison with the results obtained for Sn-doped ZnS nanopowders [9]. The crystallite size decreased linearly with the increase in Sn concentration in thin films while the crystallite size was found to increase with the increase in Sn concentration in nanopowders.

3.2 Morphological Studies

Figure 2a–d shows the EDAX spectra of the $Zn_{1-x}Sn_xS$ thin films at different Sn concentrations. The insets of the figures are the corresponding FE-SEM micrographs of the films. From the SEM images, it is clear that the films are of smooth surface with uniform grains. The average grain size of the samples was greater than that of the crystallite sizes calculated from XRD. This is due to the fact that
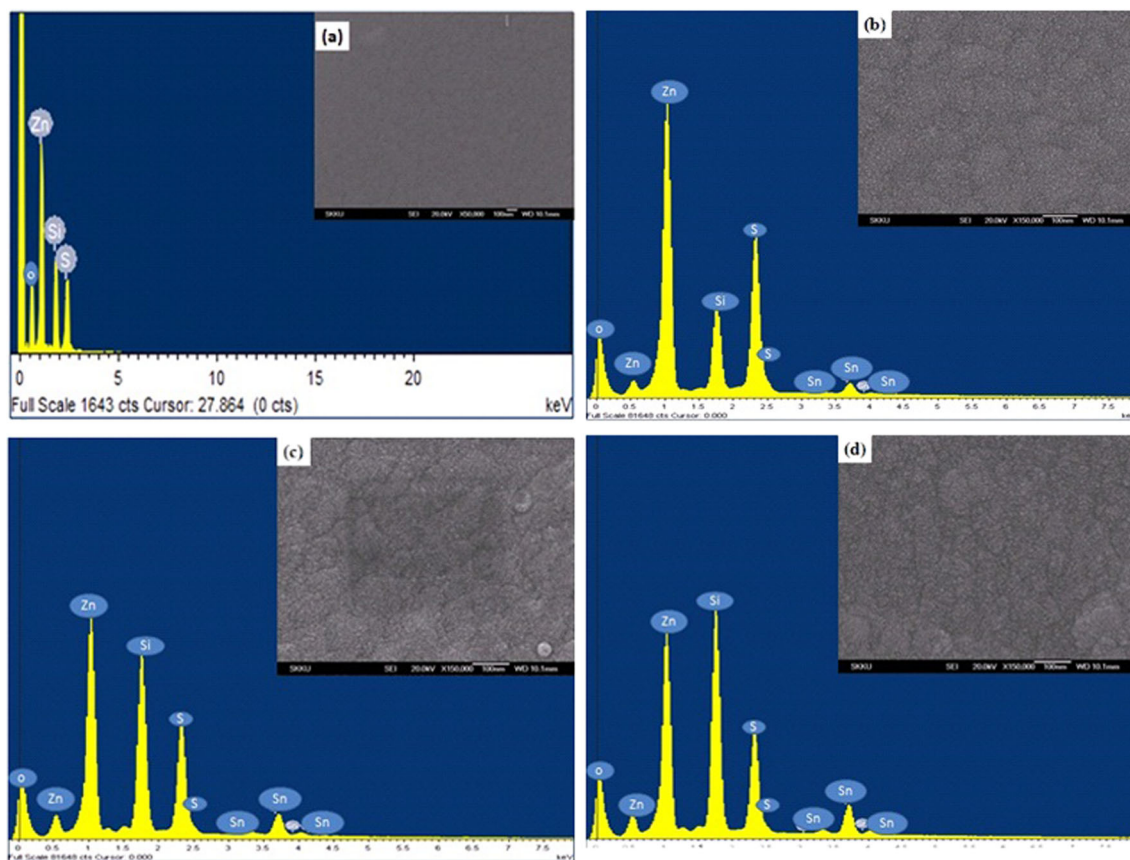

Fig. 2 EDAX images of $Zn_{1-x}Sn_xS$ thin films with FE-SEM images, **a** $x = 0.00$, **b** $x = 0.02$, **c** $x = 0.05$, and **d** $x = 0.08$

Table 2 The atomic percentage of $Zn_{1-x}Sn_xS$ thin films from EDAX

$Zn_{1-x}Sn_xS$	Zn (at%)	S (at%)	Sn (at%)	Total (at%)
$x = 0.00$	66.69	33.31	0	100
$x = 0.02$	65.60	32.78	1.62	100
$x = 0.05$	63.32	33.01	3.67	100
$x = 0.08$	61.90	31.61	6.49	100

grains consist of many crystallites [18, 19]. From the EDAX spectra, it is confirmed that no new elements were present in the films. The elements such as zinc, tin, sulfur, and oxygen were present in the films. A peak related to silicon (Si) at 1.8 eV was also observed in the spectra which is due to glass substrate effect. The atomic percentage of the elements such as zinc (Zn), tin (Sn), and sulfur (S) in thin films are shown in Table 2. The films were nearly in stoichiometric ratio.

3.3 Optical Properties

Figure 3 shows the absorption spectra of $Zn_{1-x}Sn_xS$ thin films at different Sn doping concentrations. No significant change in absorbance spectra was found with the increase of doping concentration. The absorbance was high at a wavelength of 300 nm and it decreased at higher wavelengths (400 to 800 nm).

Figure 4 shows the optical transmittance spectra of $Zn_{1-x}Sn_xS$ thin films at different Sn doping concentrations. All the films exhibited optical transmittance of more than 85% in the visible region of the solar spectrum. Due to its high transmittance in the visible region, these films will be highly useful as a window layer in solar cell applications [20].
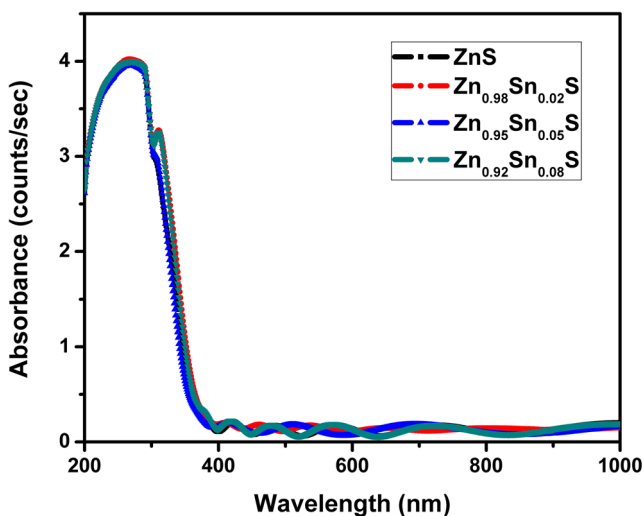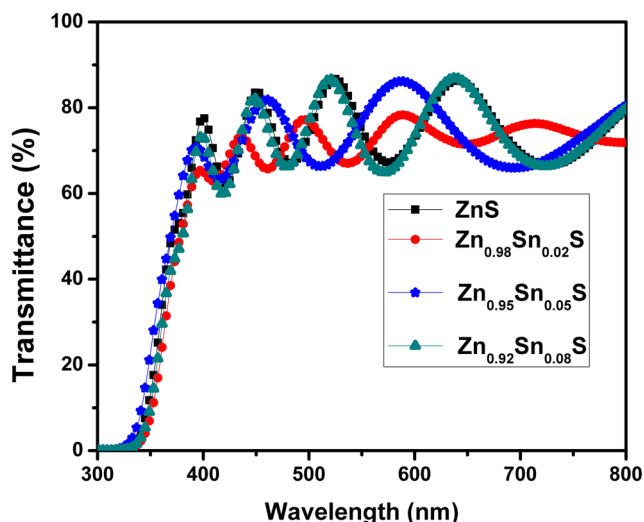

Fig. 4 Optical transmittance spectra of $Zn_{1-x}Sn_xS$ thin films

Figure 5 shows the optical band gap of the $Zn_{1-x}Sn_xS$ thin films at different Sn doping concentrations. The optical transmittance and absorbance spectra were used in calculating the optical band gap of the $Zn_{1-x}Sn_xS$ thin films. The optical band gap of the films was calculated using Tauc's relation.

$$\alpha h\nu = \left(h\nu - E_g\right)^n \qquad (4)$$

where α is the absorption coefficient, $h\nu$ is the photon energy (eV), and E_g is the optical band gap energy (eV). The n is constant which will have value $\frac{1}{2}$ for direct allowed transition and 2 for indirect allowed transition. The pure
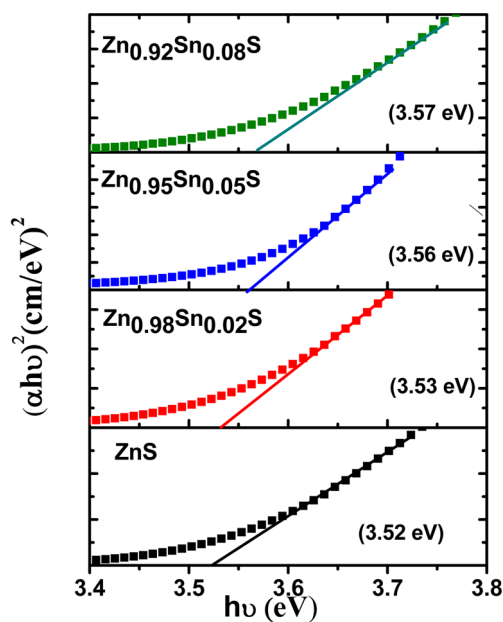

Fig. 3 Optical absorbance spectra of $Zn_{1-x}Sn_xS$ thin films at different x values

Fig. 5 Optical band gap values of $Zn_{1-x}Sn_xS$ thin films at different x values

ZnS thin films showed a band gap of 3.52 eV, and it increased with the increase of doping concentration from $x = 0.02$ to $x = 0.08$. The highest band gap of 3.57 eV was observed for the $Zn_{1-x}Sn_xS$ thin films at $x = 0.08$. The reason for the increase in optical band gap might be the decrease in crystallite size and the Burstein–Moss effect [21]. As per the Burstein–Moss effect, the Fermi energy levels merge into the conduction band by increasing carrier concentration. Hence, the lower-energy transitions will be blocked, thereby widening the band gap. As the dopant concentration increased, more and more donor states might be created which shift the Fermi level to higher energy levels. However, the band gaps observed here are lesser than that of the band gap of bulk ZnS. It may be structural modifications of ZnS due to the replacement or substitution of Sn ions in the place of zinc ions. The optical absorption coefficient (α) was determined at photon energies from transmission spectra using the Kubel-ka-Munk plot equation [22]

$$\alpha = -\frac{\ln T}{d} \tag{5}$$

where α is the absorption coefficient, d is the film thickness, and T is the optical transmittance.

The refractive index (n) and extinction coefficient (k) of $Zn_{1-x}Sn_xS$ films at $x = 0.00, 0.02, 0.05$, and 0.08 were calculated by the absorption and reflectance spectra. The refractive index n was calculated by using the relation [23]. The variation in n value with wavelength (λ) is shown in Fig. 6.
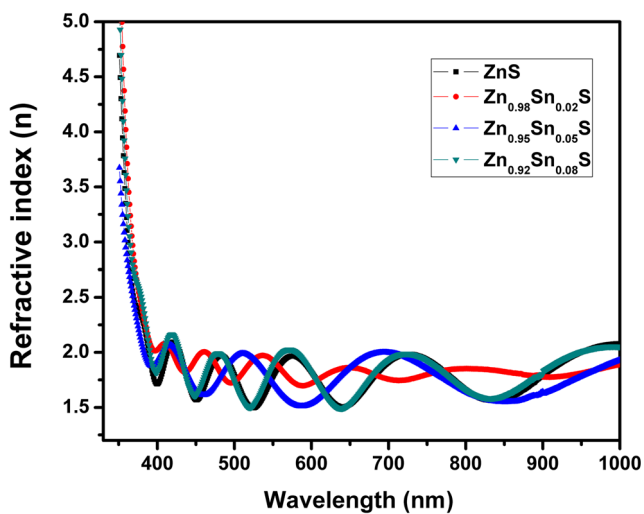
$$n = \frac{1 + \sqrt{R}}{1 - \sqrt{R}} \tag{6}$$

The reflectance R value was calculated by using (7).

$$R = 1 - \sqrt{\frac{T}{e^{-A}}} \tag{7}$$

The absorption coefficient of thin film was calculated from the expression [24]

$$\alpha = 2.303\left(\frac{A}{t}\right) \tag{8}$$

where A is absorbance and t is the thickness of the films. The absorption coefficient α and the extinction coefficient k are related by the equation [25]

$$k = \frac{\alpha \lambda}{4\pi} \tag{9}$$

where λ is the wavelength. The variation of the extinction coefficient with wavelength is shown in Fig. 6. From Figs. 6 and 7, it was observed that both n and k decreased by increasing the wavelength. The refractive index increased by increasing the dopant concentration. It has been reported that the refractive index is related to the band gap (E_g) of the material [26, 27]. It can be seen that both E_g and n values increased by the increase in Sn dopant concentration.

Figure 8 shows the photoluminescence spectra of $Zn_{1-x}Sn_xS$ thin films recorded at room temperature at different Sn concentrations at $x = 0.00, 0.02, 0.05$, and 0.08 with an excitation wavelength of 375 nm. A broad and intense peak at 420 nm was observed in all the films, and there was no change in the peak position with the increase of Sn doping. The emission peak at 420 nm might be due to surface defects created by sulfur vacancies as reported by Pawar et al. [14] and Lu et al. [28]. The intensity of the luminescence peak decreased with the increase in the dopant concentration. The quenching of luminescence peaks indicates the decrease in the rate of recombination of
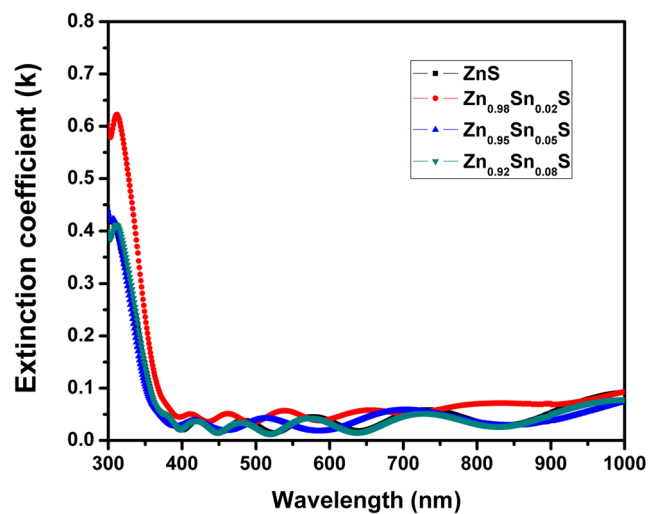

Fig. 6 Variation of the refractive index (n) with wavelength (λ) for $Zn_{1-x}Sn_xS$ thin films

Fig. 7 Variation of extinction coefficient (k) with wavelength for $Zn_{1-x}Sn_xS$ thin films
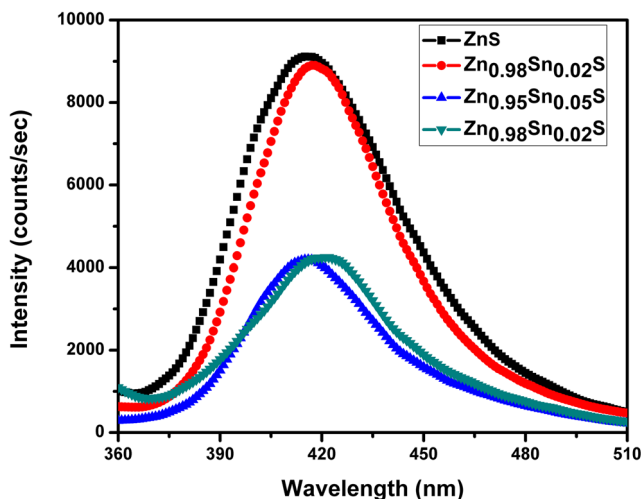
Fig. 8 Photoluminescence spectra o $Zn_{1-x}Sn_xS$ thin films

electron and hole pairs. Similar results were also observed by Mukherjee et al. [29] in Sn-doped ZnS films prepared by the chemical bath method.

3.4 Magnetic Properties

Figure 9 shows the field-dependent magnetization (M–H) curves of (a) glass substrate with $Zn_{1-x}Sn_xS$ film (x = 0.02), (b) glass substrate, and (c) $Zn_{1-x}Sn_xS$ thin film after subtracting the substrate background effect. From the figure, it is clear that the pure glass substrate exhibited a diamagnetic nature. When the ZnS films were coated onto glass substrate, they showed the paramagnetic nature. After the substrate background effect was removed, it is clear that the ZnS thin films exhibit a clear ferromagnetic nature. The effect of glass substrate on the magnetization has been removed by this method for all the $Zn_{1-x}Sn_xS$ films.
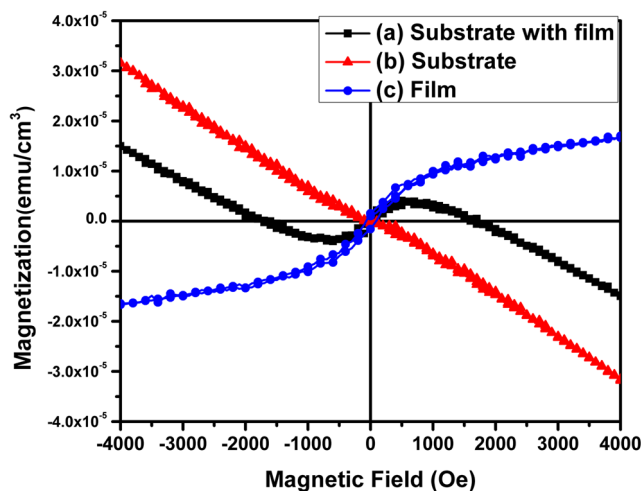
Figure 10a shows the M–H curves of $Zn_{1-x}Sn_xS$ (x = 0.00, 0.02, 0.05, and 0.08) thin films at room temperature. The diamagnetic and paramagnetic background has been removed as discussed earlier. The hysteresis loop was observed at room temperature in the applied field range of $\pm$ 6000 Oe which indicates the soft ferromagnetism in the films. In general, the bulk ZnS exhibit a diamagnetic nature. But when the crystallite size decreased to less than 2 nm, it exhibited weak ferromagnetism [9]. Further, the pure ZnS thin film exhibited weak ferromagnetism at room temperature. The –H loop of pure ZnS thin films is shown in Fig. 10a which clearly represents the soft ferromagnetism. The inset in Fig. 10a shows the ferromagnetic behavior of pure ZnS nanopowders. Similar kinds of results were found in Gd/Cr-doped ZnS nanoparticles [30, 31]. The retentivity and coercivity of the $Zn_{1-x}Sn_xS$ films increased with increasing dopant concentration from 0.00 to 0.05,
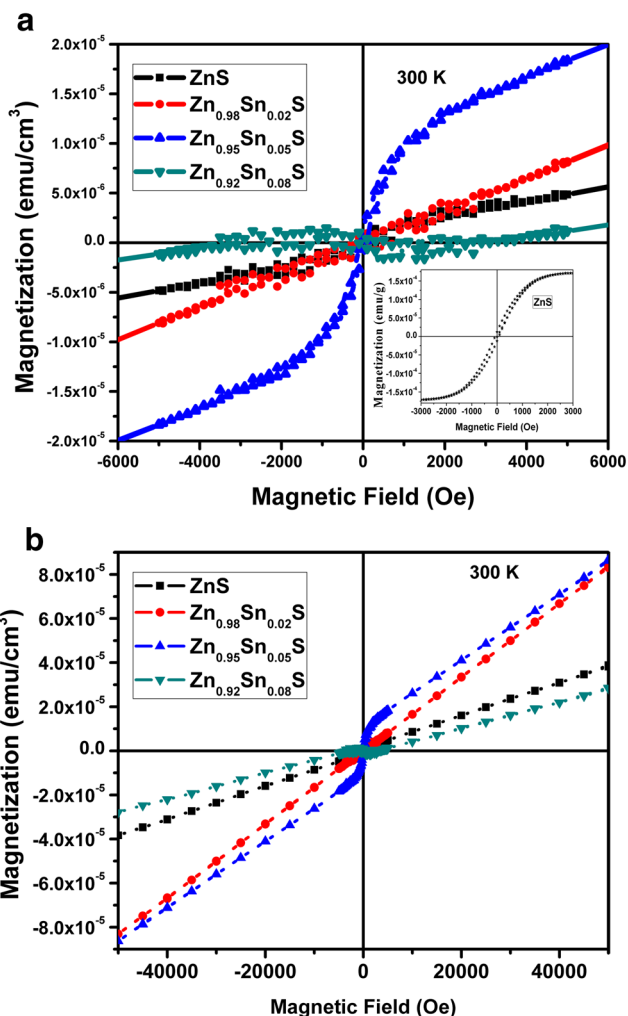

Fig. 9 M–H loops of **a** substrate with film, **b** substrate, and **c** film at 300 K in an applied field of $\pm$ 4000 Oe

Fig. 10 **a** H loops of $Zn_{1-x}Sn_xS$ thin films at 300 K under an applied field of $\pm$ 6000 Oe. **b** H loops of $Zn_{1-x}Sn_xS$ thin films at 300 K under an applied field of $\pm$ 50 kOe

Table 3 The maximum magnetization and retentivity values of $Zn_{1-x}Sn_xS$ thin films

$Zn_{1-x}Sn_xS$	Maximum magnetization M_x (µemu/cm^3)	Retentivity M_r (µemu/cm^3)
$x =$	4	0.5
$x = 0.02$	8	1.1
$x = 0.05$	18	1.6
$x = 0.08$	2	0.8

then decreased at higher Sn concentration of 0.08. The retentivity of $1.48 \ 10^-$ emu/cm3 and coercivity of 91.8 Oe were found at x 0.05. Similar kinds of weak magnetic signals were reported by many research groups [32–34], and they have correlated the signals with dopant concentration. The M–H curve at x 0.05 indicates the clear ferromagnetic behavior and the soft ferromagnetism with diamagnetic behavior at higher magnetic fields. It may be due to the spin reorientation between the SnS and ZnS dipoles. Similar results were also reported by other research groups [35, 36]. The magnetic moment increased by the increase in the doping concentration from x 0.02 to 0.05. But the

magnetic moment decreased at higher Sn concentration. The decrease in magnetic moment at higher concentration was also observed in bulk $Zn_{1-x}Sn_xS$ [9]. From Fig. 10b, all the films exhibit a paramagnetic nature under the applied field ±50,000 Oe. The summary of the data related to the M–H curve is shown in Table 3.

Earlier, superparamagnetism was reported for Sn-doped ZnS nanopowders [9]. In Sn-doped ZnS nanopowders, the spins were exhibiting superparamagnetism at room temperature, and when they are coated as a thin film, due to the high surface energy of the electrons, they exhibit weak ferromagnetism.

For further insight of magnetic properties, the temperature-dependent magnetic plots of the films were analyzed. Figure 11d shows the field-cooled (FC) and zero-field-cooled (ZFC) curves of th $Zn_{1-x}Sn_xS$ thin films. It was observed that the magnetization of both ZFC and FC decreases rapidly up to 70 K; after that, no significant change has been observed. The small difference between the ZFC and FC shows the paramagnetic behavior of the films. From the field-dependent and temperature-dependent magnetization plots, it is confirmed that the samples exhibit weak ferromagnetism at low external magnetic fields and paramagnetic nature at higher magnetic fields.
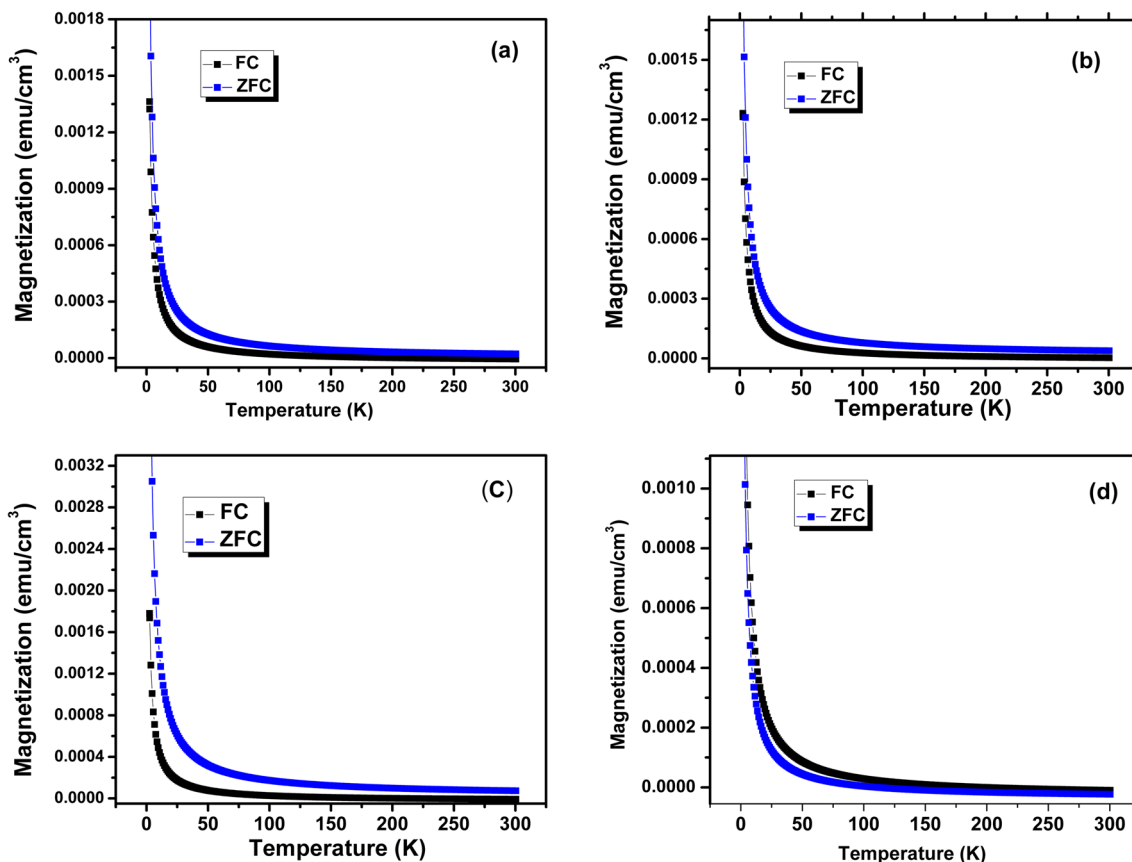
Fig. 11 ZFC and FC magnetization curves of $Zn_{1-x}Sn_xS$ thin films **a** $x = 0.00$, **b** $x = 0.02$, **c** $x = 0.05$, and **d** $x = 0.08$

4 Conclusion

Cubic-structured $Z_{n1-x}Sn_xS$ thin films were grown using the electron beam evaporation technique with an average crystallite size of 2 nm. All the thin films were almost stoichiometric in ratio. All the thin films were highly transparent (85%) with a wide band gap. Undoped and Sn-doped thin films exhibited a soft ferromagnetic nature at room temperature (300 K) and at a lower external applied magnetic field. The films showed the highest magnetization (M_s) 18×10^{-6} emu/cm^3, retentivity (M_r) 1.6×10^{-6} emu/cm^3, and coercive field (H_c) 91.80 Oe at Sn concentration $x = 0.05$. All the films exhibited a paramagnetic nature at high applied magnetic fields.

References

1. Datta, A., Panda, S.K., Chaudhuri, S.: Phase transformation and optical properties of Cu-doped ZnS nanorods. J. Solid State Chem. **181**(9), 2332–2337 (2008)
2. Fang, X., Gautam, U.K., Bando, Y., Golberg, D.: One-dimensional ZnS-based hetero-, core/shell and hierarchical nanostructures. J. Mater. Sci. Technol. **24**(4), 520 (2008)
3. Murugadoss, G., Rajamannan, B., Madhusudhanana, U.: Synthesis and characterization of water-soluble zns: Mn $^{2+}$ nanocrystals. Chalcogenide Lett. **6**(5), 197–201 (2009)
4. Yang, P., Lü, M., Xü, D., Yuan, D., Zhou, G.: Photoluminescence properties of ZnS nanoparticles co-doped with Pb 2+ and Cu 2+. Chem. Phys. Lett. **336**(1), 76–80 (2001)
5. Farid, H., Rafea, M.A., El-Wahidy, E., El-Shazly, O.: Preparation and characterization of ZnS nanocrystalline thin films by low cost dip technique. J. Mater. Sci. Mater. Electron. **25**(5), 2017–2023 (2014)
6. Mohamed, S.: Photocatalytic, optical and electrical properties of copper-doped zinc sulfide thin films. J. Phys. D. Appl. Phys. **43**(3), 035406 (2010)
7. Ortíz-Ramos, D.E., González, L.A., Ramirez-Bon, R.: P-Type transparent Cu doped ZnS thin films by the chemical bath deposition method. Mater. Lett. **124**, 267–270 (2014)
8. Öztaş, M., Bedir, M., Yazici, A.N., Kafadar, E.V., Toktamş, H.: Characterization of copper-doped sprayed ZnS thin films. Physica B **381**(1), 40–46 (2006)
9. Kumar, K.C., Rao, N.M., Kaleemulla, S., Rao, G.V.: Structural, optical and magnetic properties of Sn doped ZnS nano powders prepared by solid state reaction. Phys. B Condens. Matter **522**(Supplement C), 75–80 (2017). https://doi.org/10.1016/j.physb.2017.07.071
10. Jin, C., Kim, H., Baek, K., Lee, C.: Effects of coating and thermal annealing on the photoluminescence properties of ZnS/ZnO one-dimensional radial heterostructures. Mater. Sci. Eng. B **170**(1), 143–148 (2010)
11. Xue, S.: Effects of thermal annealing on the optical properties of Ar ion irradiated ZnS films. Ceram. Int. **39**(6), 6577–6581 (2013)
12. Zhang, Z., Shen, D., Zhang, J., Shan, C., Lu, Y., Liu, Y., Li, B., Zhao, D., Yao, B., Fan, X.: The growth of single cubic phase ZnS thin films on silica glass by plasma-assisted metalorganic chemical vapor deposition. Thin Solid Films **513**(1), 114–117 (2006)
13. Cullity, B.D.: Elements of X-Ray Diffraction. Addison-Wesley, Reading (1972)
14. Pawar, M., Nimkar, S., Nandurkar, P., Tale, A., Deshmukh, S., Chaure, S.: Effect of Sn^{2+} doping on optical properties of thiourea capped ZnS nanoparticles. Chalcogenide Lett. **7**, 139–143 (2010)
15. Prabhu, K., Kannan, S., Henry, J., Sivakumar, G., Mohanraj, K.: Undoped and metal doped ZnS nanoparticles by precipitation method. Walailak Journal of Science and Technology (WJST) **11**(9), 795–801 (2013)
16. Krishnaiah, G., Rao, N.M., Reddy, D.R., Reddy, B., Reddy, P.S.: Growth and structural properties of Zn1- xCrxTe crystals. J. Cryst. Growth **310**(1), 26–30 (2008)
17. Sarmah, K., Sarma, R., Das, H.: Structural characterization of thermally evaporated CdSe thin films. Chalcogenide Lett. **5**(8), 153–163 (2008)
18. Goktas, A., Aslan, F., Mutlu, I.H.: Annealing effect on the characteristics of La0. 67Sr0. 33MnO3 polycrystalline thin films produced by the sol–gel dip-coating process. J. Mater. Sci. Mater. Electron. **23**(2), 605–611 (2012)
19. Goktas, A., Aslan, F., Tumbul, A.: Nanostructured Cu-doped ZnS polycrystalline thin films produced by a wet chemical route: the influences of Cu doping and film thickness on the structural, optical and electrical properties. J. Sol-Gel Sci. Technol. **75**(1), 45–53 (2015)
20. Wanjala, K., Njoroge, W., Ngaruiya, J.: Optical and electrical characterization of ZnS: Sn thin films for solar cell application. Int. J. Energy Eng. **6**(1), 1–7 (2016)
21. Rao, N.M., Mallikarjuna, P., Sivasankar, J., Begam, M.R.: Structural, Optical and Magnetic Properties of Cu Doped ZnSe Powders. Chemtech (2014)
22. Pankove, J.I.: Optical Processes in Semiconductors. Courier Corporation, North Chelmsford (2012)
23. Hussein, H., Shabeeb, G.M., Hashim, S.S.: Preparation ZnO thin film by using sol-gel-processed and determination of thickness and study optical properties. J. Mater. Environ. Sci **2**(4), 423–426 (2011)
24. Kumar, K.B., Raji, P.: Synthesis and characterization of nano zinc oxide by sol gel spin coating. Rec. Res. Sci. Technol. **3**(3), 48–52 (2011)
25. Shakti, N., Gupta, P.: Structural and optical properties of sol-gel prepared ZnO thin film. Appl. Phys. Res. **2**(1), 19 (2010)
26. Tsuchiya, T., Ozaki, S., Adachi, S.: Modelling the optical constants of cubic ZnS in the 0–20 eV spectral region. J. Phys.: Condens. Matter **15**(22), 3717 (2003)
27. Hughes, J.L., Sipe, J.: Comparison of calculated optical response in cubic and hexagonal II-VI semiconductors. Phys. Rev. B **58**(12), 7761 (1998)
28. Lu, H.-Y., Chu, S.-Y., Tan, S.-S.: The characteristics of low-temperature-synthesized ZnS and ZnO nanoparticles. J. Cryst. Growth **269**(2), 385–391 (2004)
29. Mukherjee, A., Mitra, P.: Characterization of Sn doped ZnS thin films synthesized by CBD. Mater. Res. **20**, 430–435 (2017)
30. Kaur, P., Kumar, S., Chen, C.-L., Yang, K.-S., Wei, D.-H., Dong, C.-L., Srivastava, C., Rao, S.: Gd doping induced weak ferromagnetic ordering in ZnS nanoparticles synthesized by low temperature co-precipitation technique. Mater. Chem. Phys. **186**, 124–130 (2017)
31. Kaur, P., Kumar, S., Singh, A., Chen, C., Dong, C., Chan, T., Lee, K., Srivastava, C., Rao, S., Wu, M.: Investigations on doping induced changes in structural, electronic structure and magnetic behavior of spintronic Cr–ZnS nanoparticles. Superlattices Microstruct. **83**, 785–795 (2015)
32. Zhu, F., Dong, S., Yang, G.: Ferromagnetic properties in Fe-doped ZnS thin films (2010)
33. Goktas, A., Mutlu, I.: Structural, optical, and magnetic properties of solution-processed co-doped ZnS thin films. J. Electron. Mater. **45**(11), 5709–5720 (2016)

34. Kumar, V., Saroja, M., Venkatachalam, M., Shankar, S.: Structural, optical and magnetic properties of ZnS, MZS & CZS thin films prepared by sol-gel spin coating method. Thin Film Tech. **93**, 39409–34411 (2016)

35. Mala, N., Ravichandran, K., Pandiarajan, S., Srinivasan, N., Ravikumar, B., Pushpa, K.C.S., Swaminathan, K., Arun, T.: Formation of hexagonal plate shaped ZnO microparticles—a study on antibacterial and magnetic properties. Ceram. Int. **42**(6), 7336–7346 (2016)

36. Ganeshraja, A.S., Thirumurugan, S., Rajkumar, K., Zhu, K., Wang, Y., Anbalagan, K., Wang, J.: Effects of structural, optical and ferromagnetic states on the photocatalytic activities of Sn–TiO 2 nanocrystals. RSC Adv. **6**(1), 409–421 (2016)